

MRAC-Based Voltage Controller for Three-Phase CVCF Inverters to Attenuate Parameter Uncertainties Under Critical Load Conditions

Jinuk Kim¹, Han Ho Choi¹, Member, IEEE, and Jin-Woo Jung¹, Member, IEEE

Abstract—This paper investigates a robust model reference adaptive control (MRAC) method for a three-phase constant-voltage constant-frequency (CVCF) inverter with an output *LC* filter. The proposed MRAC method is designed to stabilize the error dynamics of the system by a feedback control term in the steady state and attenuate the parameter uncertainties of the system by an updated MRAC term. Unlike the conventional proportional-derivative control (PDC) scheme, the proposed MRAC scheme ensures the fast convergence of the output errors to the exponential trajectories predefined by the reference models. Furthermore, the adaptive state-feedback mechanism can guarantee the fast dynamic response in the transient state without using load current sensors or observers. The asymptotic stability is mathematically proven by a Lyapunov theory. The feasibility of the proposed controller is confirmed through extensive experimental studies on a prototype three-phase CVCF inverter with a TI TMS320LF28335 DSP. Finally, comparative experimental results of three control methods (i.e., conventional PDC, feedback linearization control, and proposed MRAC) are provided to validate the superior performance of the proposed method such as fast transient response, low total harmonic distortion, and robustness to parameter uncertainties under critical load conditions (i.e., abrupt load changes, unbalanced loads, and distorted nonlinear loads).

Index Terms—Constant-voltage constant-frequency (CVCF) inverter, model reference adaptive control (MRAC), three-phase inverter, total harmonic distortion (THD), voltage control.

I. INTRODUCTION

IN RECENT years, three-phase constant-voltage constant-frequency (CVCF) inverters have been widely used because of the rapidly increasing demand in various applications, such as distributed generation systems, uninterruptible power supplies, and energy storage systems [1]–[3]. In these applications, the main control performance requirements of the three-phase CVCF inverters are summarized as follows: small steady-state errors (SSEs), low total harmonic distortion (THD), and fast dynamic response at the output voltages regardless of the load

Manuscript received February 25, 2019; accepted April 16, 2019. Date of publication April 21, 2019; date of current version October 18, 2019. This work was supported by the Basic Science Research Program through the National Research Foundation of Korea funded by the Ministry of Education under Grant 2018R1D1A1B07046873. Recommended for publication by Associate Editor R. Kennel. (Corresponding author: Jin-Woo Jung.)

The authors are with the Division of Electronics and Electrical Engineering, Dongguk University (Seoul), Seoul 04620, South Korea (e-mail: jinwjung@dongguk.edu).

Color versions of one or more of the figures in this paper are available online at <http://ieeexplore.ieee.org>.

Digital Object Identifier 10.1109/TPEL.2019.2912393

conditions, such as abrupt load changes, unbalanced loads, and nonlinear loads. Furthermore, the CVCF inverters should be robust against the disturbances such as load disturbances, system parameter uncertainties, and measurement noises [4]–[6]. However, in order to achieve all the aforementioned requirements, there are difficulties in the CVCF inverter control owing to the following constraints: the system parameter uncertainties and variations, nonlinearities of the power devices and *LC* filters, and highly distorted loads. Therefore, a good voltage controller design of the three-phase CVCF inverter system is needed to overcome these constraints and satisfy the above-mentioned control requirements under critical load conditions, such as unbalanced loads and distorted nonlinear loads [7], [8].

Of late years, numerous research works have been continuously published to achieve the above-mentioned control requirements with both linear control schemes [9]–[19] and nonlinear control schemes [20]–[34]. First, the linear control methods, such as proportional–integral (PI) control [9], [10], proportional–derivative (PD) control [11], linear quadratic regulator (LQR) [12], [13], proportional–resonant (PR) control [14]–[16], and repetitive control (RC) [17], [18], are widely applied in practical applications. The PI and PD control schemes achieve simple and easy implementations and good performance in the steady state. The LQR performance is enhanced by using the particle swarm optimization algorithm [12] and unified control structure for both α and β axes [13]. However, the transient performance is not guaranteed owing to the lack of robustness in the case of parameter uncertainties [9]–[13]. Next, the PR control [14], [15] is more robust compared to other control schemes because of the good response characteristics at a resonant frequency and zero SSE by introducing the infinite gain. However, this control scheme has stability problems because of the infinite gain around resonant frequency, and slow dynamic performance in load-step compensation [16]. In addition, the RC scheme [17], [18] originating from the internal model principle is known as an effective solution for eliminating the periodic errors in a dynamic system. However, this scheme has shortcomings such as slow dynamics, large memory requirements, and poor transient responses in the presence of nonperiodic disturbances [19].

Second, the nonlinear control methods have been reported, such as sliding mode control (SMC) [20], model predictive control (MPC) [21], [22], feedback linearization control (FLC) [23]–[25], and adaptive control [26], [27]. The SMC scheme is found to be robust against bounded parameter uncertainties,

but it suffers from the fixed coefficients utilized in the sliding surface function, which limits the dynamic response of the closed-loop system [20]. Next, the MPC scheme has attracted researchers recently owing to its salient features such as an easy inclusion of the nonlinear constraints [21], [22]. However, its performance highly depends on the precise knowledge of the model parameters, which is not always available. In [23], the FLC scheme is designed to achieve low THD under nonlinear loads. However, this control scheme has a complex design structure and high computational burden for its implementation [24], [25].

Among nonlinear control schemes, the adaptive control scheme is a powerful tool because of its advantages such as robustness against system parameter uncertainties and good transient performance under nonlinear loads [26]. However, this approach needs at once complicated computations and observers to achieve accurate values of the load currents [27]. In [28]–[34], it is worth mentioning that a model reference adaptive control (MRAC) is an attractive control method because despite the lack of the information about the systems, the MRAC scheme stabilizes the error dynamics and achieves the fast dynamic response by tracking a specified reference model using an adaptive control law. Thus, it has been successfully implemented in various applications including motor control [28], [29], robot manipulation [30], unmanned underwater vehicles [31], and aircraft control [32]. Despite the advantages of the MRAC, there are few research works in the literature that apply the MRAC to the voltage control of the three-phase CVCF inverter systems with an output *LC* filter. Also, the majority of MRAC-based methods tried to estimate the parameters of the plant such as equivalent resistance and reactance in the three-phase CVCF inverter systems [33], [34] and rotor and stator resistances in the motor drives [28], [29]. Then, the estimated values are used to adjust the controller parameters that obtain the desired transient response. It means that the MRAC-based method to estimate the model parameters are indirectly used in the control law.

This paper proposes a robust MRAC scheme for the three-phase CVCF inverter systems with an *LC* filter. The proposed MRAC law can be divided into the following two main terms: a feedback control (FC) term and an updated MRAC term. The first term stabilizes the system error dynamics by a feedback manner to achieve an acceptable voltage tracking in the steady state. Next, the second term is designed to attenuate the system parameters' uncertainties that significantly degrade the voltage regulation [35], [36] by using the reference voltage models. Unlike other control schemes, such as linear control schemes [9]–[19] and nonlinear control schemes [20]–[34], the proposed method can be used for various practical applications because it does not require any accurate knowledge about system parameters without using the load current sensors or observers. In addition, the proposed MRAC can guarantee the fast convergence of the output errors to the exponential trajectories predefined by the reference models. Then, the asymptotic stability of the proposed MRAC is mathematically proven by a Lyapunov function. Therefore, the proposed scheme can assure acceptable voltage

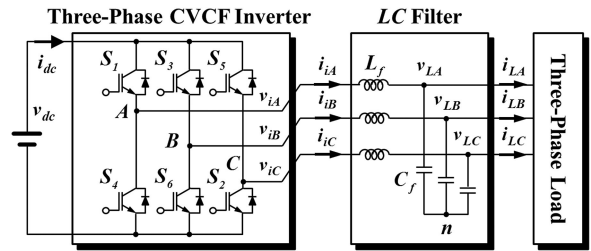


Fig. 1. Topology of a three-phase CVCF inverter system with an *LC* filter.

tracking behaviors such as small SSE, low THD, fast transient response, and robustness to parameter uncertainties under critical load conditions such as load step change, unbalanced load, and distorted nonlinear load. The comparative experimental results on a prototype three-phase CVCF inverter system with a TI TMS320F28335 floating point DSP are presented under severe load conditions (i.e., load step change, unbalanced load, and distorted nonlinear load) in the presence of the model parameter uncertainties. Finally, it is validated that the proposed MRAC scheme has an excellent voltage regulation performance in comparison with the conventional PD control (PDC) scheme and FLC scheme.

II. DYNAMIC MODEL FOR A THREE-PHASE CVCF INVERTER SYSTEM

The three-phase CVCF inverter system with an output *LC* filter is depicted in Fig. 1, which is composed of a dc-link voltage (v_{dc}), a three-phase inverter (i.e., S_1 – S_6), an output *LC* filter (i.e., L_f and C_f), and a three-phase load (e.g., linear or nonlinear load). Also, the circuit diagram in Fig. 1 uses the following quantities: the inverter output line to neutral voltage vector $\mathbf{V}_{iABC} = [v_{iA}, v_{iB}, v_{iC}]^T$, load line to neutral voltage vector $\mathbf{V}_{LABC} = [v_{LA}, v_{LB}, v_{LC}]^T$, inverter phase current vector $\mathbf{I}_{iABC} = [i_{iA}, i_{iB}, i_{iC}]^T$, and load phase current vector $\mathbf{I}_{LABC} = [i_{LA}, i_{LB}, i_{LC}]^T$.

In this paper, the mathematical model of the three-phase inverter in the synchronously rotating d – q reference frame is obtained by applying *Kirchhoff's voltage law* and *current law* to the *LC* filter via *Park's* and *Clarke's transformations* as the following equations [25], [26]:

$$\begin{cases} \dot{i}_{id} = \omega i_{iq} + k_2 v_{id} - k_2 v_{Ld} \\ \dot{i}_{iq} = -\omega i_{id} + k_2 v_{iq} - k_2 v_{Lq} \\ \dot{v}_{Ld} = \omega v_{Lq} + k_1 i_{id} - k_1 i_{Ld} \\ \dot{v}_{Lq} = -\omega v_{Ld} + k_1 i_{id} - k_1 i_{Lq} \end{cases} \quad (1)$$

where $k_1 = 1/C_f$ and $k_2 = 1/L_f$, ω is the angular frequency ($\omega = 2\pi f$), and f is the fundamental frequency. Also, v_{id} and v_{iq} are the dq -axis control inputs, v_{Ld} and v_{Lq} are the dq -axis load voltages, i_{id} and i_{iq} are the dq -axis inverter currents, and i_{Ld} and i_{Lq} are the dq -axis load currents.

By using the reference voltages (v_{dr} and v_{qr}) and voltage errors (v_{de} and v_{qe}), the dynamic model of a three-phase CVCF

inverter can be rewritten as follows [12]:

$$\begin{cases} \dot{i}_{id} = \omega i_{iq} + k_2 v_{id} - k_2 v_{de} - k_2 v_{dr} \\ \dot{i}_{iq} = -\omega i_{id} + k_2 v_{iq} - k_2 v_{qe} - k_2 v_{qr} \\ \dot{v}_{Ld} = \dot{v}_{de} = \omega v_{qe} + \omega v_{qr} + k_1 i_{id} - k_1 i_{Ld} \\ \dot{v}_{Lq} = \dot{v}_{qe} = -\omega v_{de} - \omega v_{dr} + k_1 i_{id} - k_1 i_{Lq} \end{cases} \quad (2)$$

where $v_{de} = v_{Ld} - v_{dr}$, $v_{qe} = v_{Lq} - v_{qr}$, and $\dot{v}_{dr} = \dot{v}_{qr} = 0$.

The voltage error dynamics are represented with the following first-order derivatives of the state variables:

$$\begin{cases} \dot{x}_1 = x_2 \\ \dot{x}_2 = \omega x_4 + k_1 \dot{i}_{id} \\ = \omega x_4 - k_1 k_2 x_1 - k_1 k_2 v_{dr} + \omega k_1 i_{iq} + k_1 k_2 v_{id} \\ \dot{x}_3 = x_4 \\ \dot{x}_4 = -\omega x_2 + k_1 \dot{i}_{iq} \\ = -\omega x_2 - k_1 k_2 x_3 - k_1 k_2 v_{qr} - \omega k_1 i_{id} + k_1 k_2 v_{iq} \end{cases} \quad (3)$$

where $x_1 = v_{de}$, $x_2 = \dot{v}_{de}$, $x_3 = v_{qe}$, $x_4 = \dot{v}_{qe}$, and $i_{Ld} = i_{Lq} = 0$.

The second-order derivatives of the dq -axis voltage errors can be calculated directly from the control inputs (v_{id} and v_{iq}) as follows:

$$\dot{x}_2 = k_1 k_2 (v_{id} + d_d), \quad \dot{x}_4 = k_1 k_2 (v_{iq} + d_q) \quad (4)$$

where d_d and d_q are the disturbances of the voltage error dynamics given by

$$\begin{cases} d_d = -x_1 + \frac{\omega}{k_1 k_2} x_4 - v_{dr} + \frac{\omega}{k_2} i_{iq} \\ d_q = -\frac{\omega}{k_1 k_2} x_2 - x_3 - v_{qr} - \frac{\omega}{k_2} i_{id} \end{cases} \quad (5)$$

Note that the dq -axis voltage error dynamics (4) are simplified with a second-order decoupled dynamic model. Also, this model conversion allows a direct control design for v_{id} and v_{iq} to regulate v_{de} and v_{qe} without any time delay owing to an additional current loop, so the cascaded control structure can be avoided to achieve a faster dynamic response.

III. MRAC LAW DESIGN AND STABILITY ANALYSIS

This section first presents the nonadaptive control scheme named as compensated PDC (CPDC) scheme and then proposes the MRAC scheme and its stability analysis. Note that the nonadaptive control scheme is an intermediate voltage controller to design the proposed MRAC scheme.

A. Nonadaptive Control Law Design

This section deals with the nonadaptive control law (i.e., CPDC law) design of a three-phase CVCF inverter system under the assumption that parameter values (e.g., L_f , C_f , i_{Ld} , and i_{Lq}) are known.

To make the errors between the reference model output and system output converge to zero, the reference models of the closed-loop dynamics are chosen as the predefined second-order system as follows.

$$\begin{cases} \ddot{v}_{dm} + 2\lambda_d \dot{v}_{dm} + \lambda_d^2 v_{dm} = 0 \\ \ddot{v}_{qm} + 2\lambda_q \dot{v}_{qm} + \lambda_q^2 v_{qm} = 0 \end{cases} \quad (6)$$

where $\lambda_{dq} = [\lambda_d, \lambda_q]^T > 0$ are the control parameter gains and $\mathbf{V}_{dqm} = [v_{dm}, v_{qm}]^T$ are the outputs of the reference voltage models that have the exponential decay form as follows:

$$\begin{cases} v_{dm}(t) = \{[\dot{v}_{dm}(0) + \lambda_d v_{dm}(0)] t + v_{dm}(0)\} e^{-\lambda_d t} \\ v_{qm}(t) = \{[\dot{v}_{qm}(0) + \lambda_q v_{qm}(0)] t + v_{qm}(0)\} e^{-\lambda_q t} \end{cases} \quad (7a)$$

Let us define $\dot{v}_{dm}(0) = -\lambda_d v_{dm}(0)$ and $\dot{v}_{qm}(0) = -\lambda_q v_{qm}(0)$, so the reference models (7a) can be reduced to the following simple decay form:

$$\begin{cases} v_{dm} = v_{dm}(0) e^{-\lambda_d t} \\ v_{qm} = v_{qm}(0) e^{-\lambda_q t} \end{cases} \quad (7b)$$

Note that the error convergence rates are directly defined by the control parameter gains (λ_{dq}) shown in (7b). Also, the exponential decay of the output errors is defined by intuitively referring to the reference voltage models \mathbf{V}_{dqm} in (7b). Therefore, in order to realize the fast convergence of \mathbf{V}_{dqm} with stiff dynamics within 1/10th of the sampling time (T_s), the control parameter gains (λ_{dq}) are tuned to large values [25]. However, the stiff dynamics make the physical system difficult to instantly and precisely follow the reference models in the presence of the input constraints such as the limited control inputs (e.g., $|\mathbf{V}_{idq}| \leq (2/3)v_{dc}$) where $\mathbf{V}_{idq} = [v_{id}, v_{iq}]^T$ are the control inputs [37].

The voltage error dynamics (\mathbf{V}_{dqe}) and model reference dynamics (\mathbf{V}_{dqm}) are compared by using the newly defined error variables (i.e., $\mathbf{E}_{dq} = [e_d, e_q]^T$) as

$$\begin{cases} e_d = v_{de} - v_{dm} \\ e_q = v_{qe} - v_{qm} \end{cases} \quad (8)$$

Then, the second-order derivatives of the error dynamics (\mathbf{E}_{dq}) can be obtained by using (4), (6), and (8) as follows:

$$\begin{cases} \ddot{e}_d = k_1 k_2 \left(v_{id} + d_d + \frac{2\lambda_d}{k_1 k_2} \dot{v}_{dm} + \frac{\lambda_d^2}{k_1 k_2} v_{dm} \right) \\ \ddot{e}_q = k_1 k_2 \left(v_{iq} + d_q + \frac{2\lambda_q}{k_1 k_2} \dot{v}_{qm} + \frac{\lambda_q^2}{k_1 k_2} v_{qm} \right) \end{cases} \quad (9)$$

As mentioned above, if the specific parameters of the three-phase CVCF inverter system are known, in order to make the error (\mathbf{E}_{dq}) converge to zero, the nonadaptive control law (i.e., CPDC law) can be established by the following:

$$\begin{cases} v_{id} = \underbrace{-\kappa_d \sigma_d}_{v_{id_FC}} + \underbrace{v_{Ld}}_{v_{id_CC}} + \underbrace{\psi_d^{*T} h_d}_{v_{id_NACC}} \\ v_{iq} = \underbrace{-\kappa_q \sigma_q}_{v_{iq_FC}} + \underbrace{v_{Lq}}_{v_{iq_CC}} + \underbrace{\psi_q^{*T} h_q}_{v_{iq_NACC}} \end{cases} \quad (10)$$

where $\kappa_{dq} = [\kappa_d, \kappa_q]^T > 0$ are the feedback coefficients, $-\kappa_d \sigma_d$ and $-\kappa_q \sigma_q$ are the FC terms (i.e., v_{id_FC} and v_{iq_FC}), v_{Ld} and v_{Lq} are the feedforward compensation control (CC) terms (i.e., v_{id_CC} and v_{iq_CC}), $\psi_d^{*T} h_d$ and $\psi_q^{*T} h_q$ are the nonadaptive CC (NACC) terms (i.e., v_{id_NACC} and v_{iq_NACC}), and σ_d and σ_q are the tracking error dynamics.

The parameters of the NACC terms ($\psi_d^{*T} h_d$ and $\psi_q^{*T} h_q$) include the following constant parameter vectors $\psi^* = [\psi_d^*, \psi_q^*]^T$:

$$\begin{cases} \psi_d^* = \left[-\frac{\lambda_d}{k_1 k_2}, -\frac{\omega}{k_1 k_2}, -\frac{\omega}{k_2}, -\frac{\lambda_d}{k_1 k_2}, -\frac{\lambda_d^2}{k_1 k_2} \right]^T \\ \psi_q^* = \left[\frac{\omega}{k_1 k_2}, -\frac{\lambda_q}{k_1 k_2}, \frac{\omega}{k_2}, -\frac{\lambda_q}{k_1 k_2}, -\frac{\lambda_q^2}{k_1 k_2} \right]^T \end{cases} \quad (11)$$

and the system parameter vectors $H_{dq} = [h_d, h_q]^T$ are given by

$$\begin{cases} h_d = [\dot{v}_{de}, \dot{v}_{qe}, i_{iq}, \dot{v}_{dm}, v_{dm}]^T \\ h_q = [\dot{v}_{de}, \dot{v}_{qe}, i_{id}, \dot{v}_{qm}, v_{qm}]^T \end{cases}. \quad (12)$$

Then, the tracking error dynamics (σ_d and σ_q) are deduced by

$$\begin{cases} \sigma_d = \dot{e}_d + \lambda_d e_d \\ \sigma_q = \dot{e}_q + \lambda_q e_q \end{cases} \quad (13)$$

where \dot{e}_d and \dot{e}_q are the time derivatives of the error dynamic vector e .

Remark 1: If the reference models in (7b) are neglected (i.e., $v_{dm}(0) = v_{qm}(0) = 0$), the FC terms can be expressed as the conventional PDC terms as follows [11]:

$$\begin{cases} v_{id} = -\kappa_d \sigma_d = -\kappa_d (\dot{v}_{de} + \lambda_d v_{de}) \\ v_{iq} = -\kappa_q \sigma_q = -\kappa_q (\dot{v}_{qe} + \lambda_q v_{qe}) \end{cases}. \quad (14)$$

Note that the conventional PDC scheme (14) increases the stability of the system because of the P control terms (i.e., $\kappa_d \lambda_d v_{de}$ and $\kappa_q \lambda_q v_{qe}$), which has an ability to predict the future error of the system response by the D control terms (i.e., $\kappa_d \dot{v}_{de}$ and $\kappa_q \dot{v}_{qe}$) [9], [10]. However, this control scheme (14) may show a poor control performance such as large time delay process and susceptibility to disturbances [11]. To overcome these limitations, the nonadaptive control law (i.e., CPDC law) in (10) allows a flexible choice of the whole reference dynamics by adding the CC terms (v_{Ld} and v_{Lq}) to make up for the voltage errors and NACC terms ($\psi_d^{*T} h_d$ and $\psi_q^{*T} h_q$) to guarantee the fast convergence of the output errors to the conventional PDC terms (σ_d and σ_q). In addition, the reference models (\mathbf{V}_{dqm}) in (8) can make the dynamic performance faster and more stable than the conventional PDC scheme (14). Fig. 2(a) and (b) shows the control block diagrams in order to clearly highlight the difference between the conventional PDC scheme (14) and CPDC scheme (10) by adding ① [reference models (7b)] and ② [CC + NACC terms in (10)] to the conventional PD controller for a three-phase CVCF inverter system where $\kappa\sigma = [\kappa_d \sigma_d, \kappa_q \sigma_q]^T$, $\mathbf{V}_{dqr} = [v_{dr}, v_{qr}]^T$, $\mathbf{V}_{Ldq} = [v_{Ld}, v_{Lq}]^T$, and $\mathbf{V}_{dqe} = [v_{de}, v_{qe}]^T$.

B. MRAC Law Design and Stability Analysis

The constant parameter vectors (11) of the NACC terms ($\psi_d^{*T} h_d$ and $\psi_q^{*T} h_q$) can be theoretically used to obtain the aforementioned control terms in (10). However, the precise values of the LC parameters are unavailable in practice. Therefore, this paper proposes a new MRAC law without requiring any accurate information about the LC parameters (L_f and C_f) and load current values (i_{Ld} and i_{Lq}).

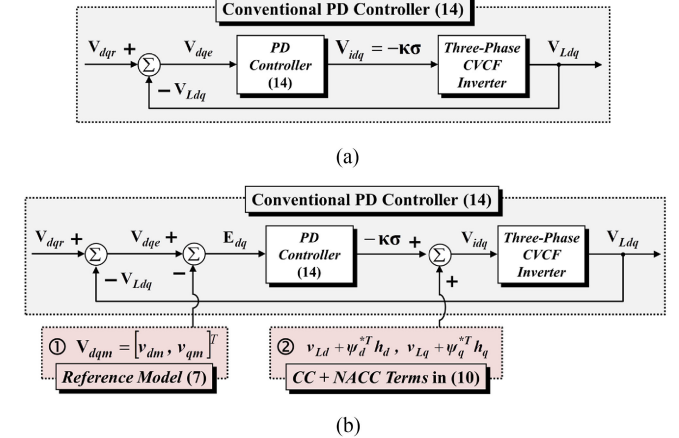


Fig. 2. Control block diagrams for a three-phase CVCF inverter system. (a) Conventional PDC scheme. (b) CPDC scheme.

Theorem 1: Assume that the LC parameters (L_f and C_f) and load current values (i_{Ld} and i_{Lq}) of the three-phase CVCF inverter system (2) are unknown. Consider the proposed adaptive control law (i.e., MRAC law) given by the following FC terms (i.e., v_{id_FC} and v_{iq_FC}), CC terms (i.e., v_{id_CC} and v_{iq_CC}), and updated MRAC terms (i.e., v_{id_MRAC} and v_{iq_MRAC}) as follows:

$$\begin{cases} v_{id} = \underbrace{-\kappa_d \sigma_d}_{v_{id_FC}} + \underbrace{v_{Ld}}_{v_{id_CC}} + \underbrace{\hat{\psi}_d^T h_d}_{v_{id_MRAC}} \\ v_{iq} = \underbrace{-\kappa_q \sigma_q}_{v_{iq_FC}} + \underbrace{v_{Lq}}_{v_{iq_CC}} + \underbrace{\hat{\psi}_q^T h_q}_{v_{iq_MRAC}} \end{cases} \quad (15)$$

where $\hat{\psi} = [\hat{\psi}_d, \hat{\psi}_q]^T$ are an estimate value of ψ^* given by the following update law:

$$\begin{cases} \dot{\hat{\psi}}_d = -\Phi_d^{-1} h_d^T \sigma_d \\ \dot{\hat{\psi}}_q = -\Phi_q^{-1} h_q^T \sigma_q \end{cases}. \quad (16)$$

The 5×5 matrices $\Phi_d = \text{diag}(\phi_{d1}, \phi_{d2}, \phi_{d3}, \phi_{d4}, \phi_{d5})$ and $\Phi_q = \text{diag}(\phi_{q1}, \phi_{q2}, \phi_{q3}, \phi_{q4}, \phi_{q5})$ are the adaptation gains that determine the performance of the proposed adaptive control law (15). Then, $\mathbf{E}_{dq} = [e_d, e_q]^T$ converges to zero and $\hat{\psi} = [\hat{\psi}_d, \hat{\psi}_q]^T$ is bounded.

Proof: The stability of the proposed MRAC system can be analyzed in the similar manner with [38]. Let us define the Lyapunov function as follows:

$$V(t) = \frac{1}{2} \left(\sigma_d^2 + \sigma_q^2 + k_1 k_2 \tilde{\psi}_d^T \Phi_d \tilde{\psi}_d + k_1 k_2 \tilde{\psi}_q^T \Phi_q \tilde{\psi}_q \right) \quad (17)$$

where the control parameter vectors of the error dynamics are defined as $\tilde{\psi}_d = \psi_d^* - \hat{\psi}_d$ and $\tilde{\psi}_q = \psi_q^* - \hat{\psi}_q$.

Then, the time derivative of $V(t)$ can be expressed as

$$\begin{aligned} \frac{dV}{dt} &= \frac{1}{2} \left(2\sigma_d \frac{d\sigma_d}{dt} + 2k_1 k_2 \tilde{\psi}_d^T \Phi_d \frac{d\tilde{\psi}_d}{dt} \right) \\ &\quad + \frac{1}{2} \left(2\sigma_q \frac{d\sigma_q}{dt} + 2k_1 k_2 \tilde{\psi}_q^T \Phi_q \frac{d\tilde{\psi}_q}{dt} \right) \end{aligned} \quad (18)$$

or

$$\begin{aligned} \frac{dV}{dt} &= \sigma_d \dot{\sigma}_d + \sigma_q \dot{\sigma}_q \\ &+ k_1 k_2 \left\{ \tilde{\psi}_d^T \Phi_d \left(\dot{\psi}_d^* - \dot{\hat{\psi}}_d \right) + \tilde{\psi}_q^T \Phi_q \left(\dot{\psi}_q^* - \dot{\hat{\psi}}_q \right) \right\}. \end{aligned} \quad (19)$$

By using (13), the time derivative of $V(t)$ can be established by the following:

$$\begin{aligned} \frac{dV}{dt} &= \sigma_d (\ddot{\sigma}_d + \lambda_d \dot{\sigma}_d) + \sigma_q (\ddot{\sigma}_q + \lambda_q \dot{\sigma}_q) \\ &+ k_1 k_2 \left(\tilde{\psi}_d^T h_d \sigma_d + \tilde{\psi}_q^T h_q \sigma_q \right). \end{aligned} \quad (20)$$

The above equations (19) and (20) imply that

$$\begin{aligned} \dot{V} &= \sigma_d \dot{\sigma}_d + \sigma_q \dot{\sigma}_q + k_1 k_2 \left(\tilde{\psi}_d^T h_d \sigma_d + \tilde{\psi}_q^T h_q \sigma_q \right) \\ &= -k_1 k_2 (\kappa_d \sigma_d^2 + \kappa_q \sigma_q^2) \leq 0. \end{aligned} \quad (21)$$

Integrating both sides of (21) gives

$$\int_0^\infty \dot{V}(\tau) d\tau \leq -k_1 k_2 \left(\kappa_d \int_0^\infty \sigma_d^2 d\tau + \kappa_q \int_0^\infty \sigma_q^2 d\tau \right). \quad (22)$$

Thus, the aforementioned inequality can be rewritten as

$$\begin{aligned} k_1 k_2 \left(\kappa_d \int_0^\infty \sigma_d^2 d\tau + \kappa_q \int_0^\infty \sigma_q^2 d\tau \right) \\ \leq V(0) - V(\infty) \leq V(0) \end{aligned} \quad (23)$$

where $V(t) \geq 0$ is used. Then, the following inequality can be derived:

$$\int_0^\infty \sigma_d^2 d\tau < \infty, \quad \int_0^\infty \sigma_q^2 d\tau < \infty \quad (24)$$

which implies that $\sigma_d, \sigma_q \in L_2$. Since $\dot{V} \leq 0$, as shown in (21) and (23), $V(t)$ is nonincreasing and upper bounded as $V(t) \leq V(0)$. This implies that $\sigma_d, \sigma_q, \hat{\psi}_d$, and $\hat{\psi}_q$ are bounded as $\sigma_d \in L_\infty, \sigma_q \in L_\infty, \hat{\psi}_d \in L_\infty$, and $\hat{\psi}_q \in L_\infty$. Then, the transfer functions $G_d(s)$ from σ_d to e_d and $G_q(s)$ from σ_q to e_q are given by the following strictly positive real functions:

$$G_d(s) = \frac{1}{s + \lambda_d}, \quad G_q(s) = \frac{1}{s + \lambda_q}. \quad (25)$$

Therefore, from (13) and [38], it can be concluded that the error (E_{dq}) converges to zero in the steady state.

Remark 2: Generally, if the adaptation gains (Φ_d and Φ_q) are large, the adaptation speed is slow and the transient tracking error is large, so the adaptation gains are tuned as follows: First, increase the adaptation gains to make the controlled outputs converge faster, and then slowly decrease these values until a satisfactory transient performance is achieved [26], [27]. The proposed MRAC method ensures the fast convergence of the output errors to the exponential trajectories predefined by the reference models (7b). Furthermore, the proposed control law (15) does not require any accurate knowledge about system parameters without using the load current sensors or observers and achieves the fast dynamic response in the transient state.

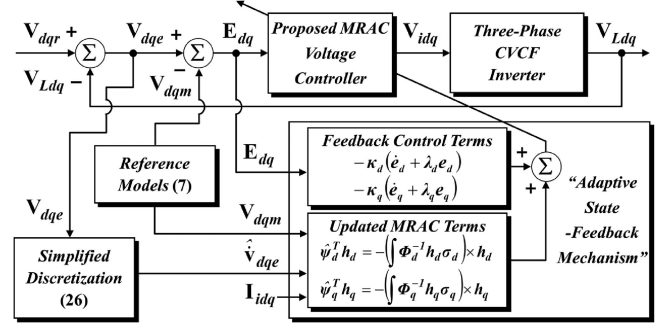


Fig. 3. Overall block diagram of the proposed MRAC-based voltage controller for a three-phase CVCF inverter system with an LC filter.

Remark 3: Note that the proposed control law (15) requires the information of the time derivatives of the load voltages ($\dot{v}_{de} = \dot{v}_{Ld} - \dot{v}_{dr}$ and $\dot{v}_{qe} = \dot{v}_{Lq} - \dot{v}_{qr}$) as shown in (11) and (16). In fact, these derivative terms can be calculated directly from the load voltages, but it is so difficult to accurately obtain the derivative terms through this direct calculation owing to high-frequency noise components [25]. Therefore, the following simplified discretization method can be used to avoid this limitation mentioned above. Based on (3), the time derivatives of the load voltages are estimated by the following recursive equations [27]:

$$\begin{cases} \hat{x}_2(t) = \frac{1}{T_s + \phi_d} [v_{de}(t) - v_{de}(t - T_s)] + \frac{\phi_d}{T_s + \phi_d} \hat{x}_2(t - T_s) \\ \hat{x}_4(t) = \frac{1}{T_s + \phi_q} [v_{qe}(t) - v_{qe}(t - T_s)] + \frac{\phi_q}{T_s + \phi_q} \hat{x}_4(t - T_s) \end{cases} \quad (26)$$

where T_s is the sampling time and ϕ_d and ϕ_q are the sufficiently small filter constants (i.e., $0 < \phi_d$ and $\phi_q \ll 1$) to limit the vulnerability of this simplified discretization to noise. Therefore, the proposed control law (15) is simply computed without using the information of the time derivatives of the load voltages (\dot{v}_{de} and \dot{v}_{qe}) in (11) and (16). Fig. 3 shows the overall block diagram of the proposed MRAC-based voltage controller for a three-phase CVCF inverter system with an LC filter where $\hat{v}_{dqe} = [\hat{v}_{de}, \hat{v}_{qe}]^T$ and $\mathbf{I}_{idq} = [i_{id}, i_{iq}]^T$.

Considering the inevitable delay in the voltage controller, the design procedure for the proposed MRAC-based voltage controller (15) is summarized to obtain the control inputs (v_{id} and v_{iq}) as follows.

- Step 1: Build the system model (1) in the synchronously rotating $d-q$ reference frame.
- Step 2: Choose the design parameter gains ($\lambda_{dq} = [\lambda_d, \lambda_q]^T$) and initial values ($v_{dm}(0)$ and $v_{qm}(0)$) for the reference models (7b). Since the error dynamics ($E_{dq} = [e_d, e_q]^T$) are designed to follow the outputs of the reference voltage models ($\mathbf{V}_{dqm} = [v_{dm}, v_{qm}]^T$), λ_{dq} should be chosen as large values (e.g., $\lambda_d = \lambda_q = 10^4$). Then, $v_{dm}(0)$ and $v_{qm}(0)$ should be set to small values (e.g., $v_{dm}(0) = v_{qm}(0) = 10$) to design the controller with a fast dynamic response.
- Step 3: By utilizing the tuning rule of the conventional PDC method in [9]–[11], tune the feedback coefficients ($\kappa_{dq} = [\kappa_d, \kappa_q]^T$) for (10) and (15). These coefficients

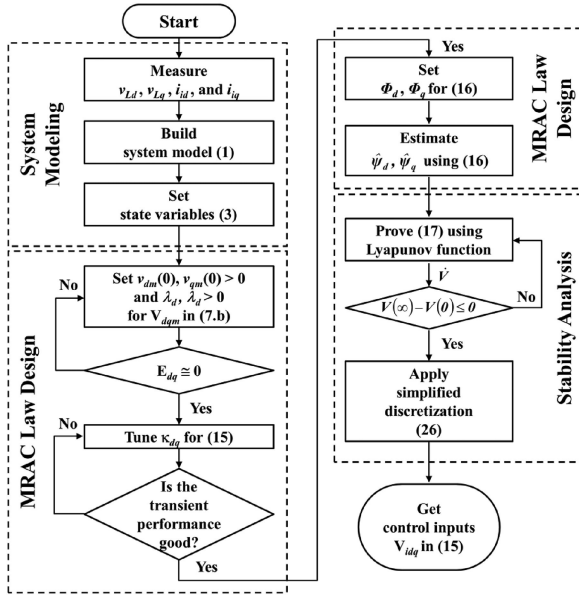


Fig. 4. Flowchart of the proposed MRAC-based voltage control algorithm for a three-phase CVCF inverter.

should be set to quite large values (e.g., $\kappa_d = \kappa_q = 2 \times 10^2$) in order to avoid a slow rising time and long settling time, and then gradually decrease the values of κ_{dq} . If the acceptable transient performance is obtained, then quit, or else, return to the start of Step 3.

Step 4: Set the adaptation gain matrices (Φ_d and Φ_q) in (16) with large values based on the tuning rules [26], [27]. These matrices assure that the control system errors converge exponentially to zero under bounded parameter conditions. Tuning these gains by a specified amount can result in an improved performance in the transient and steady states.

Step 5: Apply the simplified discretization (26) for the updated MRAC terms in (15) and (16), and then get the proposed adaptive control inputs ($\mathbf{V}_{idq} = [v_{id}, v_{iq}]^T$) (15).

Consequently, the proposed MRAC-based voltage control algorithm described earlier can be easily understood from the flowchart depicted in Fig. 4. In this figure, the flowchart illustrates the process on how to apply the adaptive laws to the system model (1) and obtain the control inputs (\mathbf{V}_{idq}) without using any load current sensors or observers to attenuate the system disturbances.

IV. EXPERIMENTAL FEASIBILITY STUDIES AND PERFORMANCE VALIDATIONS

A. Experimental Prototype Setup

In this section, simulations on MATLAB/Simulink and experiments on a prototype three-phase CVCF inverter test bed with a TI TMS320F28335 DSP are executed to verify the effectiveness of the proposed MRAC-based voltage controller. In this paper,

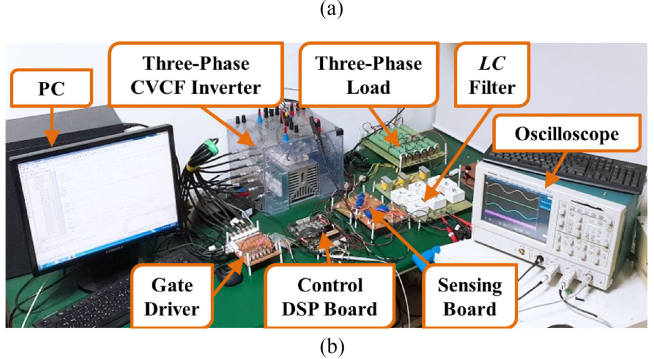
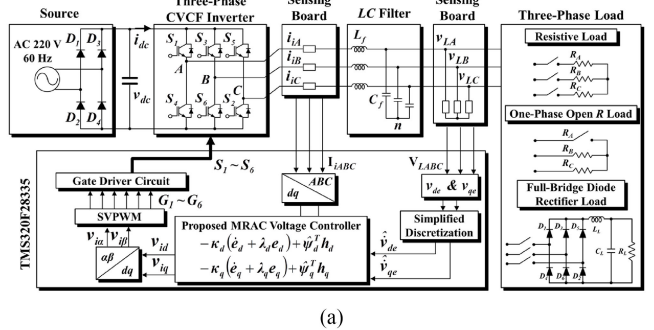


Fig. 5. Experimental setup of a prototype three-phase CVCF inverter system with an LC filter. (a) Overall schematic diagram. (b) Experimental prototype.

the conventional PDC scheme (14) and FLC scheme [23]–[25] are chosen to achieve a fair comparison because these control methods are structurally very similar to the proposed MRAC scheme (15). Fig. 5(a) and (b) presents the overall schematic diagram and experimental setup of a prototype three-phase CVCF inverter system with an LC filter, respectively.

As depicted in Fig. 5, the inverter currents ($\mathbf{i}_{ABC} = [i_{iA}, i_{iB}, i_{iC}]^T$) and load output voltages ($\mathbf{V}_{LABC} = [v_{LA}, v_{LB}, v_{LC}]^T$) are measured with the current transformers and potential transformers, and then transformed to the quantities (i_{id}, i_{iq}, v_{Ld} , and v_{Lq}) in the synchronously rotating $d-q$ reference frame.

In this paper, experiments are accomplished to demonstrate the transient and steady-state performances of the proposed MRAC-based voltage controller under the following four different cases.

- Case 1:** Sudden unbalance in the load resistance, i.e., $R_A = R_B = R_C = 50 \Omega$ to $R_A = \infty \Omega$ and $R_B = R_C = 50 \Omega$.
- Case 2:** Nonlinear load with the full-bridge diode rectifier, i.e., $R_L = 100 \Omega$, $C_L = 50 \mu\text{F}$, and $L_L = 4 \text{ mH}$.
- Case 3:** Step change in the load resistance, i.e., $R_A = R_B = R_C = \infty \Omega$ to $R_A = R_B = R_C = 50 \Omega$.
- Case 4:** Step change in the load resistance of the full-bridge diode rectifier, i.e., $R_L = \infty \Omega$ to 100Ω , $C_L = 50 \mu\text{F}$, and $L_L = 4 \text{ mH}$.

The nominal parameters of an experimental test bed are shown in Table I. In this paper, the values of L_f and C_f are chosen based on the tradeoff between performance and cost, i.e., the larger values of L_f and C_f lead to an improved control performance but more expensive cost [25], [26].

TABLE I
NOMINAL SYSTEM PARAMETERS FOR EXPERIMENTS

Parameters	Descriptions	Values
v_{dc}	dc-link voltage	290 V
T_s	Sampling time	200 μ s
f_s	Switching frequency	5 kHz
f_l	Fundamental frequency	60 Hz
v_{rms}	Load output voltage (rms value)	110 V
R_A, R_B, R_C	Resistance for linear load	50 Ω
L_{f0}	Output filter inductance	10 mH
C_{f0}	Output filter capacitance	6.67 μ F
R_L	Resistance for nonlinear load	100 Ω
C_L	Capacitance for nonlinear load	50 μ F
L_L	Inductance for nonlinear load	4 mH

B. Effectiveness Verifications of Reference Models via Extensive Simulation Studies

This section investigates the dynamic control performance of the proposed MRAC scheme that depends on the reference models to select the design parameter gains ($\lambda_{dq} = [\lambda_d, \lambda_q]^T$) through extensive simulation studies on MATLAB/Simulink when the reference voltages (i.e., $v_{dr} = 0$ V to 155.6 V and $v_{qr} = 0$ V) are step changed under no load condition [37].

First, the reference models ($\mathbf{V}_{dqm} = [v_{dm}, v_{qm}]^T$) (7b) define the desired trajectories of exponential decay output errors ($\mathbf{V}_{dqe} = [v_{de}, v_{qe}]^T$) using the relevant control parameter gains ($\lambda_d, \lambda_q > 0$). Theoretically, the larger control parameter gains (e.g., $\lambda_d = \lambda_q = 10^4$) result in the faster convergence of \mathbf{V}_{dqm} with stiff dynamics. However, it is difficult for the physical system to immediately and accurately track the reference models under the input constraints [39].

Fig. 6 indicates the reference voltage tracking performance with different control parameter gains (λ_{dq}) when the reference voltages (\mathbf{V}_{dqm}) are step changed under no load condition. As illustrated in Fig. 6, the control parameter gains (λ_{dq}) are increased from $\lambda_d, \lambda_q > 0$ based on (7b) and Step 2 so that the voltage errors ($\mathbf{V}_{dqe} = [v_{de}, v_{qe}]^T$) converge to zero more quickly during the transient state. Also, the dq -axis reference models (i.e., $\mathbf{V}_{dqm} = [v_{dm}, v_{qm}]^T$) derived from (7b) converge to zero more quickly as the control parameter gains (i.e., $\lambda_{dq} = [\lambda_d, \lambda_q]^T$) increase. That is, it can be seen that the recovery times in Fig. 6(a) and (b) for obtaining a sinusoidal load voltage are above 10 ms, whereas the recovery times in Fig. 6(c) and (d) are below 2 ms. However, as shown in Fig. 6(d), the overshoot and voltage dip in the transient state can be observed when $\lambda_d, \lambda_q > 10^4$. This phenomenon represents the limitations of the real physical system (i.e., a three-phase CVCF inverter system with an LC filter) to follow the reference models. Therefore, the appropriate control parameter gains in this paper are obtained with $\lambda_d = \lambda_q = 5 \times 10^3$ for the proposed MRAC law (15) as shown in Fig. 6(c).

C. Comparative Experimental Performance With Nominal Parameters Under Different Load Conditions

In order to demonstrate the superior performance of the proposed MRAC scheme, this section shows the comparative experimental results between the conventional PDC scheme, FLC

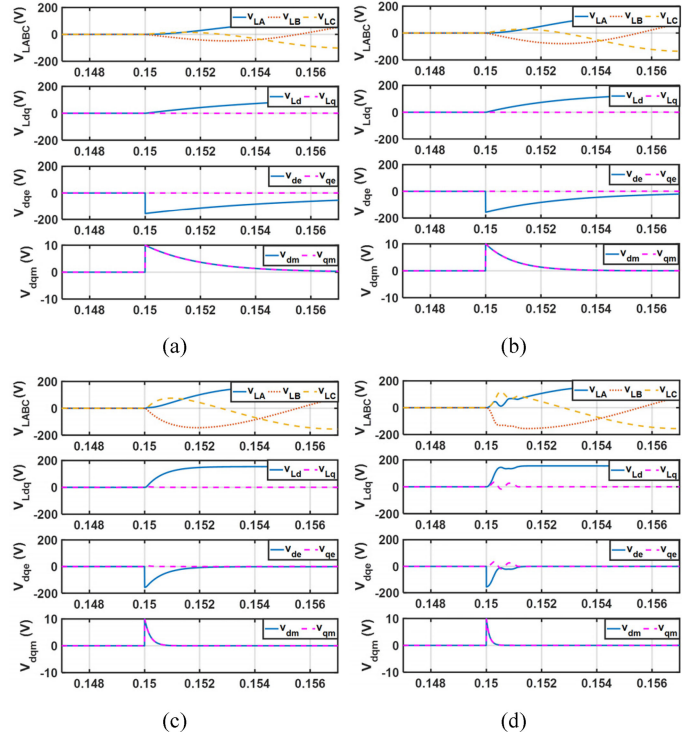


Fig. 6. Simulation results of the load voltages (\mathbf{V}_{Ldq}), voltage errors (\mathbf{V}_{dqe}), and reference models (\mathbf{V}_{dqm}) with different control parameter gains (λ_{dq}) when the reference voltage is step changed under no load condition. (a) $\lambda_d = \lambda_q = 5 \times 10^2$. (b) $\lambda_d = \lambda_q = 10^3$. (c) $\lambda_d = \lambda_q = 5 \times 10^3$. (d) $\lambda_d = \lambda_q = 10^4$.

scheme, and proposed MRAC scheme with the control parameter gains ($\lambda_d = \lambda_q = 5 \times 10^3$) under different load conditions. To perform a fair comparison, the feedback coefficients ($\kappa_{dq} = [\kappa_d, \kappa_q]^T$) of the three voltage controllers are chosen as $\kappa_d = \kappa_q = 0.2963 \times 10^{-3}$ by utilizing the tuning rule in [9]–[11]. Also, the adaptation gains (Φ_d and Φ_q) of the proposed MRAC scheme are chosen as $\Phi_d = \Phi_q = 10^4$ by utilizing the adaptation tuning rule in [26], [27]. Figs. 7–9 show the comparative experimental results of the three different control schemes with nominal parameters under Cases 1–3, respectively. Each figure shows the waveforms of the load voltages ($\mathbf{V}_{LABC} = [v_{LA}, v_{LB}, v_{LC}]^T$), load currents ($\mathbf{I}_{LABC} = [i_{LA}, i_{LB}, i_{LC}]^T$), d -axis voltage error (v_{de}), and dc-link current (i_{dc}). In this paper, the dc-link current waveform (i_{dc}) is included to give useful information that can intuitively know the load conditions such as balanced or unbalanced load and linear or nonlinear load [40]. In addition, its root-mean-square (rms) value can be used to analyze and minimize the harmonic components of the input current [41]. For a fair comparison, the control performances in the transient and steady states are verified with the d -axis voltage error waveform ($v_{de} = v_{Ld} - v_{dr}$) instead of the d -axis error dynamics waveform ($e_d = v_{de} - v_{dm}$).

Fig. 7 shows the comparative experimental waveforms of the three control schemes under Case 1 (i.e., phase A suddenly opened). In this figure, it is known from the dc-link current waveform (i_{dc}) that the load condition is changed from the balanced load (i.e., six cycles during one period) to the unbalanced

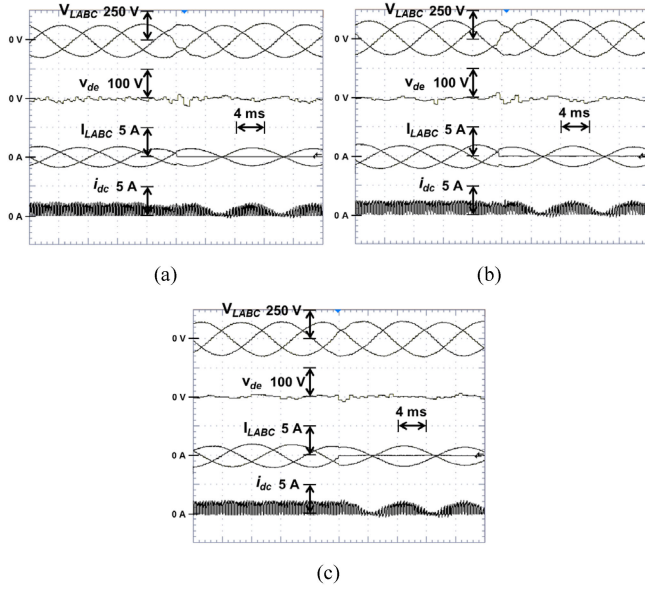


Fig. 7. Comparative experimental waveforms under Case 1 (i.e., sudden unbalance). (a) Conventional PDC scheme. (b) FLC scheme. (c) Proposed MRAC scheme.

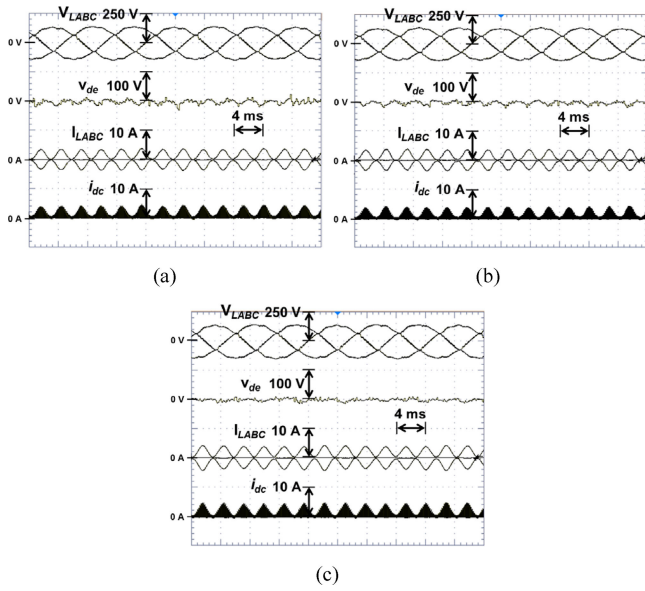


Fig. 8. Comparative experimental waveforms under Case 2 (i.e., nonlinear load with a crest factor of 2.7). (a) Conventional PDC scheme. (b) FLC scheme. (c) Proposed MRAC scheme.

load (i.e., two cycles during one period). Also, the three different voltage controllers show very fast dynamic responses at the disturbance instant with nearly no change in the output waveforms (i.e., recovered within about 2 ms). However, the proposed MRAC scheme shows the improved steady-state performance in Fig. 7(c) with reduced SSE (0.09%) and THD (0.78%) in comparison with the conventional PDC scheme (i.e., 0.45% and 1.29% in SSE and THD, respectively) shown in Fig. 7(a) and FLC scheme (i.e., 0.18% and 1.16% in SSE and THD, respectively) shown in Fig. 7(b).

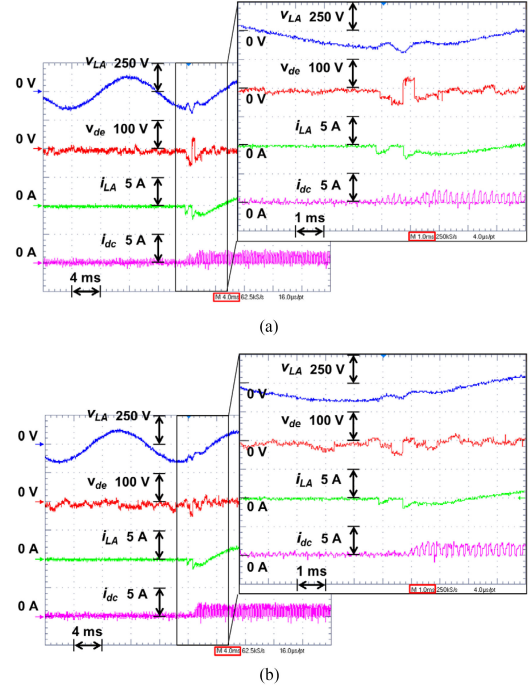


Fig. 9. Comparative experimental waveforms under Case 3 (i.e., linear load step change). (a) Conventional PDC scheme. (b) FLC scheme. (c) Proposed MRAC scheme.

Fig. 8 shows the comparative experimental waveforms of the three control schemes under Case 2 (i.e., nonlinear load with a crest factor of 2.7). In this load condition, the output waveforms of three control methods are distorted because of high-slope changes of the load currents caused by the three-phase diode rectifier. It is noted that the nonlinear load with a high crest factor of 2.7 degrades an output control performance and the more harmonic currents bring more challenging researches to achieve the high-quality output voltage of the VSI with an LC filter [42], [43]. In this case, the three different voltage controllers have to deal with the fast changes of the load currents. Fig. 8(a) and (b) shows the experimental waveforms of the conventional PDC scheme and FLC scheme with 1.91% and 1.73% in SSE and 5.32% and 3.63% in THD, respectively. Then, Fig. 8(c) shows the steady-state performance of the proposed MRAC scheme with 1.18% in SSE and 2.41% in THD.

Fig. 9 shows the comparative experimental waveforms of the three control schemes under Case 3 (i.e., linear load step change). In this figure, the three different voltage controllers

TABLE II

COMPARATIVE EXPERIMENTAL PERFORMANCE WITH NOMINAL PARAMETERS BETWEEN THE CONVENTIONAL PDC SCHEME, FLC SCHEME, AND PROPOSED MRAC SCHEME UNDER THREE DIFFERENT LOAD CONDITIONS

$\textcircled{1}$ / $\textcircled{2}$ / $\textcircled{3}$	Case 1	Case 2	Case 3
RMS Values (v_{rms})	109.5 / 109.8 / 109.9	107.9 / 108.1 / 108.7	109.1 / 109.4 / 109.7
SSE (%)	0.45 / 0.18 / 0.09	1.91 / 1.73 / 1.18	0.82 / 0.55 / 0.27
THD (%)	1.29 / 1.16 / 0.78	5.32 / 3.63 / 2.41	1.57 / 1.37 / 0.85
Recovering Time (ms)	—	—	2.3 / 2.5 / 1.1
Dip Voltage (V)	—	—	60 / 55 / 10

Note: “ $\textcircled{1}$,” “ $\textcircled{2}$,” and “ $\textcircled{3}$ ” represent the conventional PDC scheme, FLC scheme, and proposed MRAC scheme, respectively.

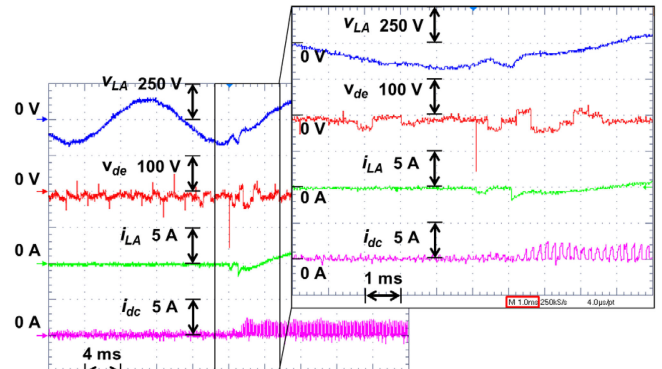
show very fast dynamic responses under a linear load step change (i.e., recovered within about 2.5 ms). However, the proposed MRAC scheme indicates the improved steady-state performance in Fig. 9(c) with reduced SSE (0.27%) and THD (0.85%) compared with the conventional PDC scheme (i.e., 0.82% and 1.57% in SSE and THD, respectively) in Fig. 9(a) and FLC scheme (i.e., 0.55% and 1.37% in SSE and THD, respectively) in Fig. 9(b).

Table II provides the comparative experimental performance between the three control schemes under different load conditions. From all experimental results and Table II, it can be concluded that the proposed MRAC scheme can attain an acceptable voltage regulation performance (i.e., lower THD in Case 2, and faster recovering time and less voltage dip in Case 3) in the transient and steady states than the conventional PDC scheme and FLC scheme under three load conditions.

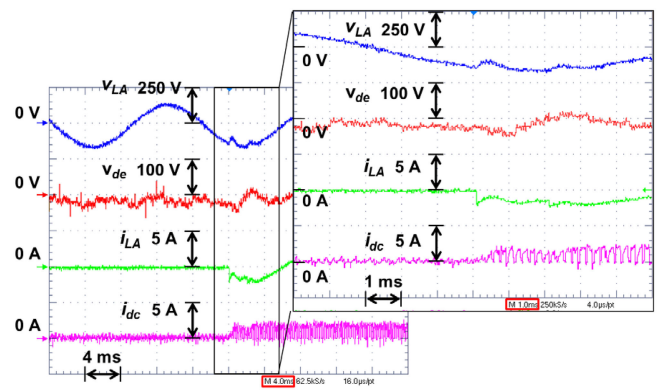
D. Robustness With Parameter Uncertainties Under the Linear and Nonlinear Load Step Changes

This section proves the robustness of the proposed MRAC scheme against parameter uncertainties by comparing the conventional PDC scheme and FLC scheme under the load step changes (i.e., Cases 3 and 4). To evaluate the robustness against the parameter uncertainties, the values of L_f and C_f are set in the control algorithm program with $\pm 40\%$ significant distortions (i.e., $\Delta L_f = +40\%$ of L_{f0} and $\Delta C_f = -40\%$ of C_{f0} ; $L_f = L_{f0} + \Delta L_f = 1.4 \times 10 = 14 \text{ mH}$ and $C_f = C_{f0} + \Delta C_f = 0.6 \times 6.67 = 4.0 \mu\text{F}$). It is noted that the parameters in the control system are mainly changed to evaluate the control robustness because this method can avoid degrading of the filtering performance owing to the physical changes in an output LC filter [44].

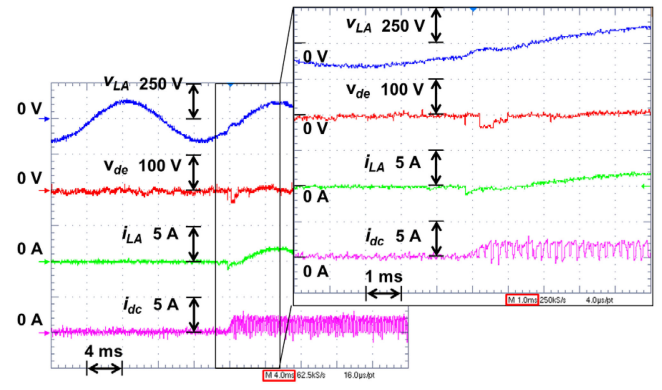
Fig. 10 shows the comparative experimental results of the three control schemes under Case 3 (i.e., linear load step change) with the parameter uncertainties (i.e., $\Delta L_f = +40\%$ of L_{f0} and $\Delta C_f = -40\%$ of C_{f0}). In this figure, three different voltage controllers show fast response properties with the recovering time within about 3 ms under a linear load step change in spite of the incorrect values of L_f and C_f . However, the proposed MRAC scheme in Fig. 10(c) exhibits a higher tracking accuracy with SSE (0.36%) and a faster recovery time within 1.2 ms in



(a)



(b)



(c)

Fig. 10. Comparative experimental waveforms to verify the robust performance under Case 3 (i.e., linear load step change) with $\pm 40\%$ variations in L_f and C_f . (a) Conventional PDC scheme. (b) FLC scheme. (c) Proposed MRAC scheme.

comparison with the conventional PDC scheme (i.e., 3.45% SSE and recovery time within 2.8 ms) shown in Fig. 10(a) and FLC scheme (i.e., 3.27% in SSE and recovery time within 2.6 ms) shown in Fig. 10(b). Also, the output voltage quality of the proposed MRAC is more improved with about 0.89% in THD than those of the conventional PDC scheme (i.e., 3.1% in THD) and FLC scheme (i.e., 2.86% in THD).

Fig. 11 shows the comparative experimental results of the three control schemes under Case 4 (i.e., nonlinear load

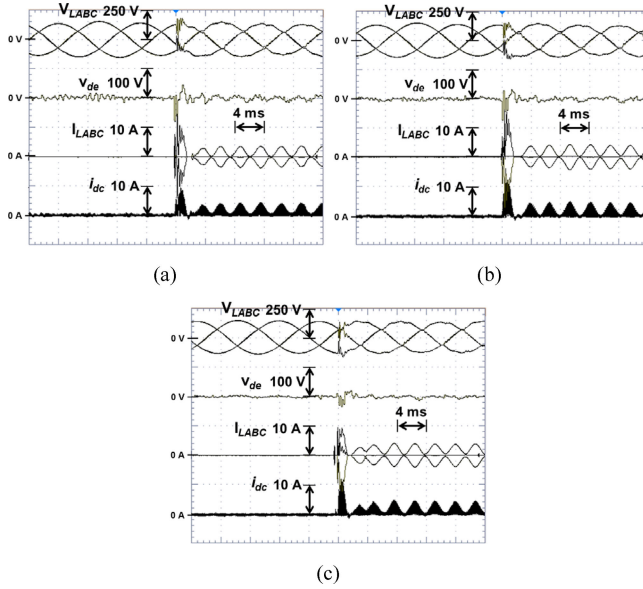


Fig. 11. Comparative experimental waveforms to verify the robust performance under Case 4 (i.e., nonlinear load step change) with $\pm 40\%$ variations in L_f and C_f . (a) Conventional PDC scheme. (b) FLC scheme. (c) Proposed MRAC scheme.

step change) with the parameter uncertainties (i.e., $\Delta L_f = +40\%$ of L_{f0} and $\Delta C_f = -40\%$ of C_{f0}). In this figure, the dc-link current (i_{dc}) waveform can be seen to fluctuate in size about 2.5 times when the load is suddenly changed from no load to nonlinear load. As observed from Fig. 11(c), the proposed MRAC scheme exhibits a higher tracking accuracy with SSE (1.27%) and a faster recovery time within 1.5 ms in comparison with the conventional PDC scheme (i.e., 5.64% in SSE and recovery time within 3.2 ms) shown in Fig. 11(a) and FLC scheme (i.e., 4.87% in SSE and recovery time within 2.6 ms) shown in Fig. 11(b). Moreover, the output voltage quality of the proposed MRAC is more improved with about 2.46% in THD than those of the conventional PDC scheme (i.e., 5.64% in THD) and FLC scheme (i.e., 4.87% in THD).

Fig. 12 shows the pulsewidth modulation (PWM) gate driving signal (G_1) from DSP for the switch S_1 , phase A load voltage (v_{LA}), and phase A load current (i_{LA}) in order to verify the operability of the proposed MRAC scheme for the three-phase CVCF inverter under different load conditions such as Case 2 (see Fig. 12(a)) and Case 3 (see Fig. 12(b) and (c)).

Finally, Table III summarizes the comparative transient and steady-state performances against parameter uncertainties between the conventional PDC scheme, FLC scheme, and proposed MRAC scheme under linear and nonlinear load step changes. Thus, even though the proposed MRAC scheme does not require any accurate information on the LC parameters (L_f and C_f) and load current values (i_{Ld} , i_{Lq}), it shows the better control performance (i.e., smaller SSEs, lower THDs, more robustness against the parameter uncertainties, shorter recovering time, and less voltage dip) in both the steady state and transient state in the presence of $\pm 40\%$ variations in the L_f and C_f than the conventional PDC scheme and FLC scheme.

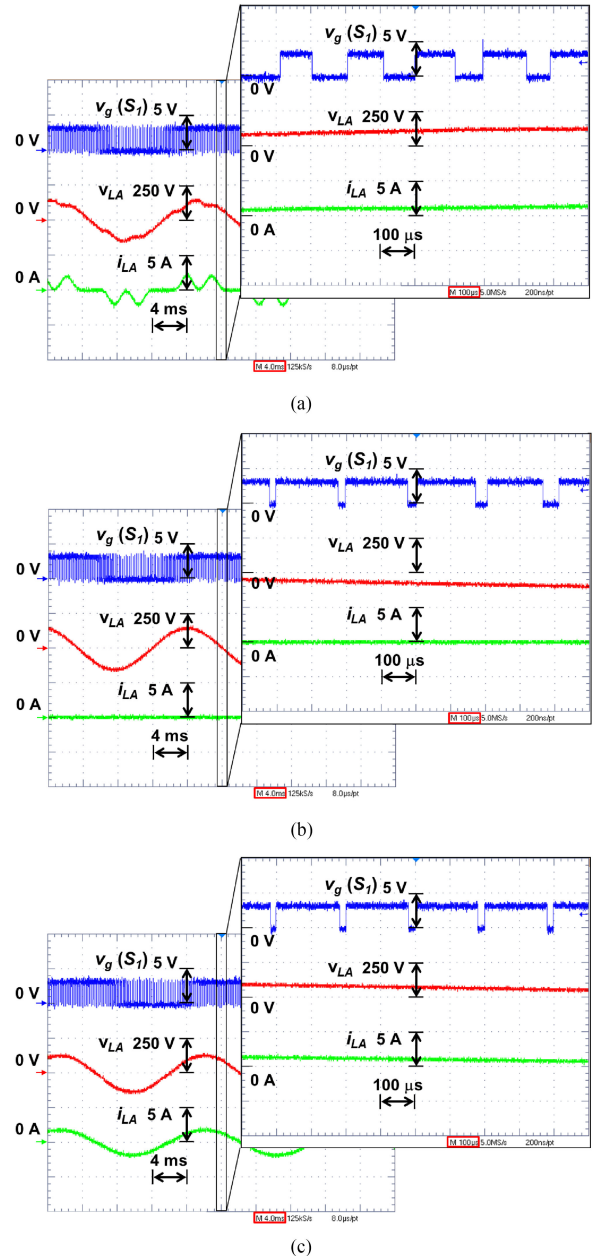


Fig. 12. PWM gate driving signal (G_1) from DSP for the switch S_1 , phase A load voltage (v_{LA}), and phase A load current (i_{LA}) of the proposed MRAC scheme under different load conditions. (a) Case 2 (Nonlinear load). (b) Case 3 (no load: before step change). (c) Case 3 (full load: after step change).

TABLE III
COMPARATIVE TRANSIENT AND STEADY-STATE PERFORMANCE AGAINST
PARAMETER UNCERTAINTIES AMONG THE CONVENTIONAL PDC SCHEME, FLC
SCHEME, AND PROPOSED MRAC SCHEME UNDER LINEAR AND NONLINEAR
LOAD STEP CHANGES

$\textcircled{1}$ / $\textcircled{2}$ / $\textcircled{3}$	Case 3	Case 4
RMS Values (v_{rms})	106.2 / 106.4 / 109.6	105.7 / 105.9 / 108.6
SSE (%)	3.45 / 3.27 / 0.36	3.91 / 3.73 / 1.27
THD (%)	3.1 / 2.86 / 0.89	5.64 / 4.87 / 2.46
Recovering Time (ms)	2.8 / 2.6 / 1.2	3.2 / 2.6 / 1.5
Dip Voltage (V)	55 / 60 / 30	63 / 55 / 35

Note: “ $\textcircled{1}$,” “ $\textcircled{2}$,” and “ $\textcircled{3}$ ” represent the conventional PDC scheme, FLC scheme, and proposed MRAC scheme, respectively.

V. CONCLUSION

This paper proposed a robust voltage controller for a three-phase CVCF inverter system with an *LC* filter based on the MRAC scheme. The proposed MRAC method has the following advantages:

- 1) precise tracking capability of the reference signals with a small SSE and a low THD;
- 2) fast dynamic response; and
- 3) less susceptible to the parameter uncertainties compared to the conventional PDC scheme and FLC scheme.

Finally, the proposed MRAC scheme verified the improved voltage regulation performance with a prototype three-phase CVCF inverter system including a TI TMS320LF28335 DSP in comparison with the conventional PDC scheme and FLC scheme under load step change, unbalanced load, and distorted nonlinear load with the *LC* parameter uncertainties.

REFERENCES

- [1] F. Nejabatkhah, Y. W. Li, and B. Wu, "Control strategies of three-phase distributed generation inverters for grid unbalanced voltage compensation," *IEEE Trans. Power Electron.*, vol. 31, no. 7, pp. 5228–5241, Jul. 2016.
- [2] M. Shahparasti, M. Mohamadian, A. Yazdian, A. A. Ahmad, and M. Amini, "Derivation of a stationary-frame single-loop controller for three-phase standalone inverter supplying nonlinear loads," *IEEE Trans. Power Electron.*, vol. 29, no. 9, pp. 506–5071, Sep. 2014.
- [3] M. Castilla, J. Miret, A. Camacho, L. G. Vicuña, and J. Matas, "Modeling and design of voltage support control schemes for three-phase inverters operating under unbalanced grid conditions," *IEEE Trans. Power Electron.*, vol. 29, no. 11, pp. 6139–6150, Nov. 2014.
- [4] Y. Yang, K. Zhou, M. Cheng, and B. Zhang, "Phase compensation multiresonant control of CVCF PWM converters," *IEEE Trans. Power Electron.*, vol. 28, no. 8, pp. 3923–3930, Aug. 2013.
- [5] B. Zhang, D. Wang, K. Zhou, and Y. Wang, "Linear phase lead compensation repetitive control of a CVCF PWM inverter," *IEEE Trans. Ind. Electron.*, vol. 55, no. 4, pp. 1595–1602, Apr. 2008.
- [6] K. Zhou and D. Wang, "Digital repetitive learning controller for three-phase CVCF PWM inverter," *IEEE Trans. Power Electron.*, vol. 48, no. 4, pp. 820–830, Aug. 2001.
- [7] Y. Wu and Y. Ye, "Internal model-based disturbance observer with application to CVCF PWM inverter," *IEEE Trans. Ind. Electron.*, vol. 65, no. 7, pp. 5743–5753, Jul. 2018.
- [8] S. Eren, M. Pahlevaninezhad, A. Bakhshai, and P. K. Jain, "Composite nonlinear feedback control and stability analysis of a grid-connected voltage source inverter with *LCL* filter," *IEEE Trans. Ind. Electron.*, vol. 60, no. 11, pp. 5059–5074, Nov. 2013.
- [9] K. S. Tang, K. F. Man, G. Chen, and S. Kwong, "An optimal fuzzy PID controller," *IEEE Trans. Ind. Electron.*, vol. 48, no. 4, pp. 757–765, Aug. 2001.
- [10] T. Chaiyatham and I. Ngamroo, "Improvement of power system transient stability by PV farm with fuzzy gain scheduling of PID controller," *IEEE Syst. J.*, vol. 11, no. 3, pp. 1684–1691, Sep. 2017.
- [11] H. Xu, A. Datta, and S. P. Bhattacharyya, "Computation of all stabilizing PID gains for digital control systems," *IEEE Trans. Autom. Control*, vol. 46, no. 4, pp. 647–652, Apr. 2001.
- [12] B. Ufnalski, A. Kaszczewski, and L. M. Grzesiak, "Particle swarm optimization of the multioscillatory LQR for a three-phase four-wire voltage-source inverter with an *LC* output filter," *IEEE Trans. Ind. Electron.*, vol. 62, no. 1, pp. 484–493, Jan. 2015.
- [13] X. Quan, Z. Wu, X. Dou, M. Hu, and A. Q. Huang, "Load current decoupling based LQ control for three-phase inverter," *IEEE Trans. Power Electron.*, vol. 33, no. 6, pp. 5476–5491, Jun. 2018.
- [14] P. C. Loh, M. J. Newman, D. N. Zmood, and D. G. Holmes, "A comparative analysis of multiloop voltage regulation strategies for single and three-phase UPS systems," *IEEE Trans. Power Electron.*, vol. 18, no. 5, pp. 1176–1185, Sep. 2003.
- [15] L. F. A. Pereira, J. V. Flores, G. Bonan, and J. M. G. da Silva, "Multiple resonant controllers for uninterruptible power supplies—A systematic robust control design approach," *IEEE Trans. Ind. Electron.*, vol. 61, no. 3, pp. 1528–1538, Mar. 2014.
- [16] X. Li, P. Lin, Y. Tang, and K. Wang, "Stability design of single-loop voltage control with enhanced dynamic for voltage-source converters with a low *LC*-resonant-frequency," *IEEE Trans. Power Electron.*, vol. 33, no. 11, pp. 9937–9951, Nov. 2018.
- [17] J. V. Flores, J. M. G. Silva, L. F. A. Pereira, and D. G. Sbarbaro, "Repetitive control design for MIMO systems with saturating actuators," *IEEE Trans. Autom. Control*, vol. 57, no. 1, pp. 192–198, Jan. 2012.
- [18] M. Abusara, S. Sharh, and P. Zanchetta, "Adaptive repetitive control with feedforward scheme for grid-connected inverters," *IET Power Electron.*, vol. 8, no. 8, pp. 1403–1410, Jul. 2015.
- [19] J. Ghosh and B. Paden, "Nonlinear repetitive control," *IEEE Trans. Autom. Control*, vol. 45, no. 5, pp. 949–954, May 2000.
- [20] X. Hao, X. Yand, T. Liu, L. Huang, and W. Chen, "A sliding-mode controller with multiresonant sliding surface for single-phase grid-connected VSI with an *LCL* filter," *IEEE Trans. Power Electron.*, vol. 28, no. 5, pp. 2259–2268, May 2013.
- [21] P. Cortés, G. Ortiz, J. I. Yuz, J. Rodríguez, S. Vazquez, and L. G. Franquelo, "Model predictive control of an inverter with output *LC* filter for UPS applications," *IEEE Trans. Ind. Electron.*, vol. 56, no. 6, pp. 1875–1883, Jun. 2009.
- [22] S. Kwak and S. K. Mun, "Model predictive control methods to reduce common-mode voltage for three-phase voltage source inverters," *IEEE Trans. Power Electron.*, vol. 30, no. 9, pp. 5019–5035, Sep. 2015.
- [23] X. Bao, F. Zhuo, Y. Tian, and P. Tan, "Simplified feedback linearization control of three-phase photovoltaic inverter with an *LCL* filter," *IEEE Trans. Power Electron.*, vol. 28, no. 6, pp. 2739–2752, Jun. 2013.
- [24] D. E. Kim and D. C. Lee, "Feedback linearization control of three-phase UPS inverter systems," *IEEE Trans. Ind. Electron.*, vol. 57, no. 3, pp. 963–968, Mar. 2010.
- [25] D. C. Lee, G. M. Lee, and K. D. Lee, "DC-bus voltage control of three-phase AC/DC PWM converters using feedback linearization," *IEEE Trans. Ind. Appl.*, vol. 36, no. 3, pp. 826–833, May/Jun. 2000.
- [26] T. D. Do, V. Q. Leu, Y. S. Choi, H. H. Choi, and J. W. Jung, "An adaptive voltage control strategy of three-phase inverter for stand-alone distributed generation systems," *IEEE Trans. Ind. Electron.*, vol. 60, no. 12, pp. 5660–5672, Dec. 2013.
- [27] S. C. Tan, Y. M. Lai, C. K. Tse, and M. K. H. Cheung, "Adaptive feed-forward and feedback control schemes for sliding mode controlled power converters," *IEEE Trans. Power Electron.*, vol. 21, no. 1, pp. 182–192, Jan. 2006.
- [28] S. Maiti, C. Chakraborty, Y. Hori, and M. C. Ta, "Model reference adaptive controller-based rotor resistance and speed estimation techniques for vector controlled induction motor drive utilizing reactive power," *IEEE Trans. Ind. Electron.*, vol. 55, no. 2, pp. 594–601, Feb. 2008.
- [29] M. E. Elbuluk, L. Tong, and I. Husain, "Neural-network-based model reference adaptive systems for high-performance motor drives and motion controls," *IEEE Trans. Ind. Appl.*, vol. 38, no. 3, pp. 879–886, May/Jun. 2002.
- [30] H. C. Cho, M. S. Fadali, K. S. Lee, and N. H. Kim, "Adaptive position and trajectory control of autonomous mobile robot systems with random friction," *IET Control Theory Appl.*, vol. 4, no. 12, pp. 2733–2742, Dec. 2010.
- [31] C. D. Makavita, S. G. Jayasinghe, H. D. Nguyen, and D. Ranmuthugala, "Experimental study of command governor adaptive control for unmanned underwater vehicles," *IEEE Trans. Control Syst. Technol.*, vol. 27, no. 1, pp. 332–345, Jan. 2019.
- [32] A. Maity, L. Höchtl, C. Heise, and F. Holzapfel, "Adaptive optimal control using frequency selective information of the system uncertainty with application to unmanned aircraft," *IEEE Trans. Cybern.*, vol. 48, no. 1, pp. 165–177, Jan. 2018.
- [33] A. Vidal, A. G. Yepes, F. D. Freijedo, J. Malvar, O. Lopez, and J. Doval-Gandoy, "A technique to estimate the equivalent loss resistance of grid-tied converters for current control analysis and design," *IEEE Trans. Power Electron.*, vol. 30, no. 3, pp. 1747–1761, Mar. 2015.
- [34] A. Vidal, A. G. Yepes, F. D. Freijedo, O. Lopez, J. Malvar, F. Baneira, and J. Doval-Gandoy, "A method for identification of the equivalent inductance and resistance in the plant model of current-controlled grid-tied converters," *IEEE Trans. Power Electron.*, vol. 30, no. 12, pp. 7245–7261, Dec. 2015.

- [35] J. S. Lim, C. Park, J. Han, and Y. I. Lee, "Robust tracking control of a three-phase DC-AC inverter for UPS applications," *IEEE Trans. Ind. Electron.*, vol. 61, no. 8, pp. 4142-4151, Aug. 2014.
- [36] Y. A. R. I. Mohamed, "Suppression of low- and high-frequency instabilities and grid-induced disturbances in distributed generation inverters," *IEEE Trans. Power Electron.*, vol. 26, no. 12, pp. 3790-3803, Dec. 2011.
- [37] H. T. Nguyen, E. K. Kim, I. P. Kim, H. H. Choi, and J. W. Jung, "Model predictive control with modulated optimal vector for a three-phase inverter with an LC filter," *IEEE Trans. Power Electron.*, vol. 33, no. 3, pp. 2690-2703, Mar. 2018.
- [38] F. L. Lewis, C. T. Abdallah, and D. M. Dawson, *Control of Robot Manipulators*. New York, NY, USA: Macmillan, 1993.
- [39] S. K. Kim, C. R. Park, T. W. Yoon, and Y. I. Lee, "Disturbance-observer based model predictive control for output voltage regulation of three-phase inverter for uninterruptible-power-supply applications," *Eur. J. Control*, vol. 23, pp. 71-83, May 2015.
- [40] X. Pei, W. Zhou, and Y. Kang, "Analysis and calculation of DC-link current and voltage ripples for three-phase inverter with unbalanced load," *IEEE Trans. Power Electron.*, vol. 30, no. 10, pp. 5401-5412, Oct. 2015.
- [41] P. A. Dahono, Y. Sato, and T. Kataoka, "Analysis and minimization of ripple components of input current and voltage of PWM inverters," *IEEE Trans. Ind. Appl.*, vol. 32, no. 4, pp. 945-950, Jul./Aug. 1996.
- [42] M. Shahparasti, M. Mohamadian, A. Yazdian, A. A. Ahmad, and M. Amini, "Derivation of a stationary-frame single-loop controller for three-phase standalone inverter supplying nonlinear loads," *IEEE Trans. Power Electron.*, vol. 29, no. 9, pp. 5063-5071, Sep. 2014.
- [43] T. Geyer and D. Quevedo, "Multistep finite control set model predictive control for power electronics," *IEEE Trans. Power Electron.*, vol. 29, no. 12, pp. 6836-6846, Dec. 2014.
- [44] M. Ghanes, M. Trabelsi, H. Abu-Rub, and L. Ben-Brahim, "Robust adaptive observer-based model predictive control for multilevel flying capacitors inverter," *IEEE Trans. Ind. Electron.*, vol. 63, no. 12, pp. 7876-7886, Dec. 2016.



Jinuk Kim received the B.S. degree in electronic engineering from Dongguk University (Seoul), Seoul, South Korea, in 2014, where he is currently working toward the Ph.D. degree with the Division of Electronics and Electrical Engineering.

His research interests include the field of electric machine drives based on microprocessor, control of distributed generation systems using renewable energy sources, and power conversion systems and drives for electric vehicles.



Han Ho Choi (M'03) received the B.S. degree in control and instrumentation engineering from Seoul National University, Seoul, South Korea, in 1988, and the M.S. and Ph.D. degrees in electrical engineering from the Korea Advanced Institute of Science and Technology, Daejeon, South Korea, in 1990 and 1994, respectively.

He is currently with the Division of Electronics and Electrical Engineering, Dongguk University (Seoul), Seoul, South Korea. His current research interests include control theory and its application to real-world problems.



Jin-Woo Jung (M'06) received the B.S. and M.S. degrees in electrical engineering from Hanyang University, Seoul, South Korea, in 1991 and 1997, respectively, and the Ph.D. degree in electrical and computer engineering from The Ohio State University, Columbus, OH, USA, in 2005.

From 1997 to 2000, he was with the Home Appliance Research Laboratory, LG Electronics Co., Ltd., Seoul, South Korea. From 2005 to 2008, he was a Senior Engineer with the R&D Center and the PDP Development Team, Samsung SDI Co., Ltd., South Korea. Since 2008, he has been a Professor with the Division of Electronics and Electrical Engineering, Dongguk University, Seoul, South Korea. His research interests include DSP-based electric machine drives, distributed generation systems using renewable energy sources, and power conversion systems and drives for electric vehicles.